



Preparation of Fe₃O₄/SiO₂/TiO₂/CeVO₄ Nanocomposites: Investigation of Photocatalytic Effects on Organic Pollutants, Bacterial Environments, and New Potential Therapeutic Candidate Against Cancer Cells

OPEN ACCESS

Edited by:

Christian Cella,
Università degli Studi G. d'Annunzio
Chieti e Pescara, Italy

Reviewed by:

Ali Maleki,
Iran University of Science and
Technology, Iran
J. Judith Vijaya,
Loyola College, India

*Correspondence:

Mahdi Rahimi-Nasrabadi
rahiminasrabadi@gmail.com
Ali Sobhani nasab
Ali.sobhaninasab@gmail.com

Specialty section:

This article was submitted to
Pharmacology of Anti-Cancer Drugs,
a section of the journal
Frontiers in Pharmacology

Received: 31 July 2019

Accepted: 10 February 2020

Published: 04 March 2020

Citation:

Marsooli MA, Rahimi-Nasrabadi M,
Fasihi-Ramandi M, Adib K,
Eghbali-Arani M, Ahmadi F, Sohoul E,
Sobhani nasab A, Mirhosseini SA,
Gangali MR, Ehrlich H and Joseph Y
(2020) Preparation of Fe₃O₄/SiO₂/
TiO₂/CeVO₄ Nanocomposites:
Investigation of Photocatalytic
Effects on Organic Pollutants,
Bacterial Environments, and New
Potential Therapeutic Candidate
Against Cancer Cells.
Front. Pharmacol. 11:192.
doi: 10.3389/fphar.2020.00192

Mohammad Amin Marsooli^{1,2}, Mahdi Rahimi-Nasrabadi^{1,2*}, Mahdi Fasihi-Ramandi^{1,2},
Kourosh Adib², Mohammad Eghbali-Arani³, Farhad Ahmadi^{4,5}, Esmail Sohoul⁶,
Ali Sobhani nasab^{7,8*}, Seyed Ali Mirhosseini¹, Mohamad Reza Gangali⁷,
Hermann Ehrlich⁹ and Yvonne Joseph⁹

¹ Applied Microbiology Research Center, Systems Biology and Poisonings Institute, Baqiyatallah University of Medical Sciences, Tehran, Iran, ² Faculty of Pharmacy, Baqiyatallah University of Medical Sciences, Tehran, Iran, ³ Department of Physics, University of Kashan, Kashan, Iran, ⁴ Physiology Research Center, Iran University of Medical Sciences, Tehran, Iran, ⁵ Department of Medicinal Chemistry, School of Pharmacy-International Campus, Iran University of Medical Sciences, Tehran, Iran, ⁶ Young Researchers and Elite Club, Science and Research Branch, Islamic Azad University, Tehran, Iran, ⁷ Social Determinants of Health (SDH) Research Center, Kashan University of Medical Sciences, Kashan, Iran, ⁸ Core Research Lab, Kashan University of Medical Sciences, Kashan, Iran, ⁹ Institute of Electronics and Sensor Materials, TU Bergakademie Freiberg, Freiberg, Germany

The new nanocomposite with various molar ratios along with magnetic properties was fabricated via precipitation (assisted by ultrasonic) procedure. The photocatalytic effects of methylene blue (~90% degradation for optimized sample in 100 min) for finding the optimized sample performed under visible light irradiation. Moreover, the photo-antibacterial impacts of bacteria culture environments were found with an optimized sample that had effective destruction of bacteria in comparison to control group. The cytotoxicity properties of panc1 cells and magnetic behaviors of the obtained nanomaterials were evaluated and its IC50 was about 500 mg/L. As an initial step, the structural, morphological and magnetic characteristics of the fabricated nanocomposites were evaluated by Fourier transform infrared spectroscopy (FT-IR), scanning electron microscopy (SEM), X-ray diffraction (XRD), energy dispersive X-ray (EDX) and MAP, UV-visible diffuse reflectance spectroscopy (DRS), and vibrating sample magnetometry (VSM) approaches. Based on SEM results, the size of nanoparticles in fabricated nanocomposite was nearly 50–70 nm for Fe₃O₄/SiO₂/TiO₂ and 80–100 nm for Fe₃O₄/SiO₂/TiO₂/CeVO₄. XRD results showed that desired nanocomposites were truly synthesized without any impurities.

Keywords: Fe₃O₄/SiO₂/TiO₂, Fe₃O₄/SiO₂/TiO₂/CeVO₄, photocatalytic, nanocomposites, photo-antibacterial, anti-cancer

INTRODUCTION

Discharge of inorganic and organic pollutants from varying industries including printing, textiles, food, and beauty products into environmental water resources has been a main environmental problem in all countries regardless of how they are developed. Up to date, different methods based on physical, chemical, and biological treatments such as membrane processes, reverse osmosis, photocatalytic degradation, photo-Fenton, ozonation, oxidation, biological, as well as electrochemical procedures have been used for remediation of industrial wastewaters (Barbusiński, 2005; Farré et al., 2005; Liu et al., 2007; Dogan and Turkdemir, 2012; Ioannou et al., 2013; Zheng et al., 2013; Suresh et al., 2014; Suresh et al., 2016; Jesudoss et al., 2017; Rajan et al., 2017; Kooshki et al., 2019; Peymani-Motlagh et al., 2019a; Peymani-Motlagh et al., 2019b; Rahimi-Nasrabadi et al., 2019; Sobhani-Nasab et al., 2019a; Sobhani-Nasab et al., 2019b; Sobhani-Nasab et al., 2019c). Among the most commonly mentioned methods which are subject to restrictions, photocatalytic degradation systems act as a smart tool, because it is simple, highly efficient, and inexpensive (Basith et al., 2014; Vijaya et al., 2017; Sedighi et al., 2018; Eghbali-Arani et al., 2018; Sobhani-Nasab et al., 2019d). Furthermore, it has an easy operation under sunlight and ambient conditions and excellent prospects for biological and chemical sensing (Lin et al., 2012) as well as has the fewer formation of disinfection byproducts. Along with to different approaches for improving the quality of water and foods against microbial agents, utilization of nanoparticles has emerged as new horizon which could contribute to antiseptic properties of several materials such as foods and water (Zhang et al., 2018). Besides the different application of NPs, anti-cancer effects of these materials have provided attractive horizon in the treatment of several cancers. Given that the utilization of NPs are related to anti-cancer impacts against a variety of malignancies (Ezhilarasi et al., 2016; Sangsefidi et al., 2017; Ezhilarasi et al., 2018). Nowadays, some of the semiconductor nanoparticles including ZnO, Dy₂Ti₂O₇, CaWO₄, CdTiO₃, NdVO₄, and TiO₂ have been considered as photocatalysis materials for purification of polluted waters (Zhang et al., 2000; Liu et al., 2014; Sobhani-Nasab and Sadeghi, 2016; Rahimi-Nasrabadi et al., 2016a; Rahimi-Nasrabadi et al., 2016b; Hosseinpour-Mashkani and Sobhani-Nasab, 2017). Titania (TiO₂) as a distinctive semiconductor-based photocatalyst has been widely applied in the field of water treatment thanks to its extraordinary properties such as low cost, availability, substantial chemical stability, chemical inertness, as well as exceptional photocatalytic behavior against degradation of organic pollutants. Also, it is environmentally friendly and has an antibacterial property (Xing et al., 2014; Ide et al., 2014).

One of the most significant aspects of a photocatalyst is bacterial inactivation property. During the irradiation of a suitable light source to photocatalyst, different reactive species like superoxide and hydroxyl radicals, as well as photogenerated electron and hole, can cause microorganisms, such as bacteria and viruses which should be deactivated (Foster et al., 2011; Basith et al., 2014; Jayaprakash et al., 2015; Jesudoss et al., 2016; Jayaprakash et al., 2017). Antibacterial activity of TiO₂ stems

from the creation of reactive oxygen species (ROS) after absorption of a photon with full energy and then, excitation of a negative charge from the valence band of TiO₂ to the conduction band. Superoxide anions ($\cdot\text{O}_2^-$) were formed after the transformation of an excited electron from the TiO₂ conduction band to oxygen molecule (Carp et al., 2004). Photoexcitation process into TiO₂ also generate holes into valence band which can oxidize some molecules such as surface absorbed H₂O and OH into extremely reactive hydroxyl radicals ($\cdot\text{OH}$) (Kim and Choi, 2002). These radicals and also other ROS diffused to the solution which surrounds the photocatalyst surface can decompose organic structures and have special antibacterial effect for titanium oxide.

However, the results of previous experiments confirm that bare TiO₂ based-nanostructure photocatalysts have weak photocatalytic performance under visible light and can experience recombination of charge carriers and a narrow light-response range, which would reasonably delay its usage in the photocatalytic operations (Kubacka et al., 2014).

To eliminate negative points about such photocatalysts, some approaches such as sensitization and combining with other semiconductors have been proposed to expand the absorption band gap of TiO₂ and reduce the possibility of recombination electron-hole in nanostructures (Subramanian et al., 2004; Hassan et al., 2019). Some introduced composites such as Ag₃PO₄/CuBi₂O₄ (Shi et al., 2017) and, Ag/AgCl/TiO₂ (Yu et al., 2009) exhibit high efficiency in photocatalytic degradation process compared to the one-component semiconductors because of development of heterojunction nanocomposite linking diverse semiconductors with corresponding band energy. With the formation of a suitable nanocomposite between semiconductors, the separation efficiency of electron-hole pairs generated accompanied by photon improves during the photocatalytic process.

Despite the good characteristics of the photocatalyst in water treatment, the lack of appropriate recovery of TiO₂ nanocomposites from treated water is a major problem when it comes to applying extensively. To overcome the problem of recovering catalytic nanoparticles from water, magnetic catalysts have been focused (Maleki and Kamalzare, 2014; Maleki et al., 2015; Maleki et al., 2016a; Maleki et al., 2016b; Maleki et al., 2017; Maleki et al., 2019b; Maleki et al., 2019c; Maleki et al., 2019a; Maleki et al., 2019d). After the water treatment process, the magnetic separation of Fe₃O₄/TiO₂ by using an external electromagnetic field recycles magnetic composites. The connection of Fe₃O₄ magnetic nanoparticles to TiO₂ photocatalytic nanoparticles have advantages of exclusive magnetic response, chemically modifiable surface, and eco-friendly (Su et al., 2014; Maleki and Kamalzare, 2014). Also, the coating of Fe₃O₄ NPs with TiO₂ prevents their massive accumulation. In addition, single Fe₃O₄ nanoparticles are susceptible and unstable under the reaction conditions and on the contrary, the interaction of Fe₃O₄ nanoparticles with TiO₂ nanoparticles causes recombination of electrons and holes and, consequently, decrease photocatalytic properties (Absalan and Nikazar, 2016). Incorporation of a layer such as a controlled silicon oxide layer between the magnetic core and photocatalyst shell can decline the negative effect of Iron oxide on the

photocatalysis process of titanium oxide, retain magnetic properties, give protection Fe₃O₄ against oxidation, and enrich the removal efficiency. Recently, a number of research has been done on the construction of recyclable photocatalytic nanocomposites of Fe₃O₄/SiO₂/TiO₂ with core-shell structure (Rashid et al., 2015). On the other hand, the malignant growth of pancreas is one of the most important causes of cancer-related death. Despite the fact that the prevalence of pancreatic cancer is much less than the breast or bowel tumor, nearly 3% of patients remain alive over five years, whereas the normal life expectancy is below 6 months (Kowalski et al., 2018).

In this study, our research group managed to synthesize Fe₃O₄/SiO₂/TiO₂/CeVO₄ (Iron oxide/silicon oxide/titanium oxide/cerium oxide) nanocomposites, and combined the advantages of heterogeneous catalysis, recycling of nanocomposite, antibacterial, and cytotoxicity activity, and enhancing of the photocatalytic property of TiO₂ photocatalyst to degrade impurities.

EXPERIMENTAL

Characterization

The morphology and size in the preparation of Fe₃O₄/SiO₂/TiO₂/CeVO₄ were accomplished through using FESEM. Fe₃O₄/SiO₂/TiO₂/CeVO₄ sonicated for 10 min. Then, 10 μL of sonicated Fe₃O₄/SiO₂/TiO₂/CeVO₄ was dropped on a copper grid and imaging was accomplished at an accelerating voltage of 200 kV. For the elemental analysis of the Fe₃O₄/SiO₂/TiO₂/CeVO₄, Energy-dispersive X-ray spectroscopy (EDX) was accomplished during SEM imaging. XRD analyses were conducted using a Philips X'pert Pro MPD with a graphite-filtered Cu Kα (k = 0.154 nm) radiation. These analyses were accomplished in a 2θ window ranging from 10° to 90°, at a 0.021 step size and 0.9 s per point measuring time. The FTIR analysis of Fe₃O₄/SiO₂/TiO₂/CeVO₄ was acquired using a Nicolet Magna-550 spectrometer and KBr pellets with scan speed of 65 spectra/s at 16 cm⁻¹. Thermal degradation or thermal stability study of Fe₃O₄/SiO₂/TiO₂/CeVO₄ were done by employing a TGA instrument with a flow rate of 30.0 ml min⁻¹ °C (Shimadzu TGA-50H). The surface area in characterization of the Fe₃O₄/SiO₂/TiO₂/CeVO₄ was accomplished on Brunauer-Emmett-Teller (BET) surface area analyzer.

Preparation of Fe₃O₄ Nanoparticles

This synthesis is based on previous work (Wei et al., 2012). The reagents of analytic grade (FeCl₃·6H₂O, FeCl₂·4H₂O, and NaOH) were used as a precursor. Generally, FeCl₃·6H₂O and FeCl₂·4H₂O with 1:2 molar ratio was dissolved in deionized water at 80 °C, and then NaOH solution (3 mol. L⁻¹) was added into the above mentioned solution dropwise under constant mechanical stirring for half an hour to reach final pH of 11. The precipitate was stirred at 80°C for 30 min, and cooled in normal temperature. Following the separation of resulted particles by a magnet, it washed frequently with deionized water and ethanol until pH of 7 was achieved. The Fe₃O₄ nanoparticles were dried at 60°C in vacuum for 8 h.

Preparation of Fe₃O₄/SiO₂ Nanocomposite

The iron oxide/silicon oxide nanocomposite was achieved by modifying the Stober process *via* the hydrolysis of tetraethyl orthosilicate (TEOS) in the presence of Fe₃O₄ nanoparticles based on the previous work (Wei et al., 2012; Abbas et al., 2014). We dispersed 0.1 g of as-synthesized Fe₃O₄ in 20 ml of water by using an ultrasonic wave. Subsequently, 2.5 ml of aqueous ammonia solution (28%) and 80 ml of ethanol were added to the mixture. Subsequent, 0.35 ml of TEOS was added dropwise into the mixed Fe₃O₄ nanoparticles under ultrasonic irradiation at room temperature. The stirring continued for half day. The separation of obtained precipitate was achieved by an external magnet and washed with water several times. Eventually, the collected precipitate was, once again, washed with water and dried in a vacuum oven at 60°C for 6 h.

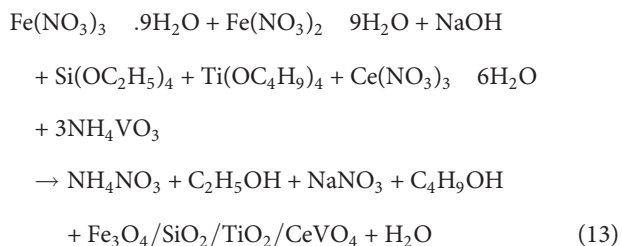
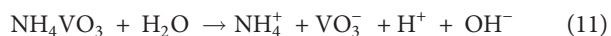
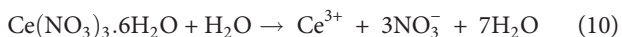
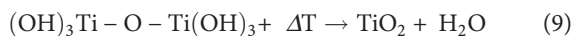
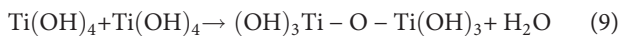
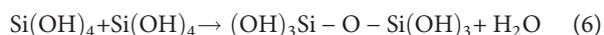
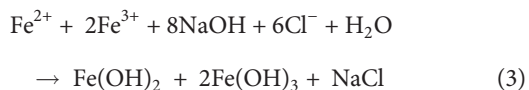
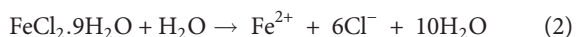
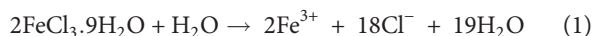
Preparation of Fe₃O₄/SiO₂/TiO₂ Nanocomposite

0.9 g of two-component iron oxide/silicon oxide nanocomposite were dispersed *via* an ultrasonic bath in 150 ml of 2-propanol for 15 min. Afterward, we added 8 ml of PEG 400 into the mixture. In the next vessel, 5 ml of tetra normal buthyl titanate (TNBT) was added to 20 ml of 12 ml of 2-propanol and 1 ml acetylacetone and stirred on a magnetic stirrer for 10 min. The second vessel was added step by step to the first mixture while it was stirring by mechanical stirrer. After 20 min, 3 ml of deionized water was added and the final mixture stirred at 70°C for 12 h. The gray precipitate of oxide/silicon oxide/titanium oxide was separated by an external magnet and washed thoroughly with ethanol and deionized water prior to drying at 60°C for 6 h and then was calcinated at 450°C for 3 h (N₁).

Preparation of Fe₃O₄/SiO₂/TiO₂/CeVO₄ Nanocomposite

To prepare the Fe₃O₄/SiO₂/TiO₂/CeVO₄ nanocomposite with 1:1:1:1 molar ratio of CeVO₄ to the previous phases, in the first container 0.371 g of non-calcinated three parts of nanocomposite, Fe₃O₄/SiO₂/TiO₂, were dispersed in 100 ml of distilled water by ultrasonic waves. Then, 0.117 g of NH₄VO₃ added to the mixture. In the second container, 0.434 g of Ce(NO₃)₃·6H₂O was dissolved in 50 ml of water. The first mixture was subjected to ultrasonic waves by a probe (400 W), and the solution of the second container was added as a dropwise to it. The reaction continued for 15 min and finally, the precipitate was washed repeatedly with deionized water as well as ethanol and dried at 60°C for 4 h. For calcination of the obtained sediments, it was placed at 450°C for 3 h (N₃). To prepare sediments with molar ratios of 1:1:1:0.5 (N₂), 1:1:1:1.5 (N₄), and 1:1:1:2 (N₅), 0.217g of Ce(NO₃)₃·6H₂O and 0.06g of NH₄VO₃, 0.65g of Ce(NO₃)₃·6H₂O and 0.176g of NH₄VO₃, and 0.87g of Ce(NO₃)₃·6H₂O and 0.234g of NH₄VO₃ were used according to the same procedure, respectively.

The reaction mechanism the Fe₃O₄/SiO₂/TiO₂/CeVO₄ nanoparticles can be proposed as following:



Photocatalytic Evaluation

In order to find the optimal sample, the photocatalytic test was performed under the visible light (assisted by H₂O₂) with 20 ppm of MB. For each test 200 mg/L of the photocatalyst was added into 0.3 L of 20 ppm MB solution. To reach improved efficiency 1 ml/100 ml of 25% H₂O₂ was added to the reaction photoreactor. In order to reach an adsorption/desorption equilibrium between catalysts and MB solution, the photoreactor container was stirred in a dark condition for 20 min prior to being subjected to the visible light source (250 W xenon lamp). Then, 4 ml of the solution were taken by a pipette and placed in dark and under light for every 10 and 20 min, respectively. Afterward, in order to separate the catalyst, it was centrifuged at 5,000 rpm for 5 min. We, eventually, evaluated the

concentration of MB through a UV-vis spectrometer to reach the outcome of photodegradation.

To analyze hydroxyl radicals which have been generated in the photocatalyst/water interface, we used the photoluminescence technique. In this procedure terephthalic acid (TA) was considered as a probe. As a result, we managed to produce 2-hydroxyterephthalic acid with highly intense fluorescence. In fact, it is the product of the TA method accompanied by hydroxyl radicals. In other words, the intensity of fluorescence is positively correlated with concentration of produced hydroxyl radicals. The set up for this test is similar to photocatalytic experiment under ultraviolet irradiation.

We prepared the reaction suspension by means of adding 0.03 g of photocatalyst (0.1 g/L) into the 300 ml aqueous solution of terephthalic acid and NaOH. The earlier and former acids were prepared with a concentration of 0.0005 M (0.451 g in 500 ml distilled water) and 0.002 M (0.04 g in 500 ml distilled water), respectively.

We utilized trapping tests of superoxide radical (O₂⁻), holes, as well as hydroxyl radical (OH), *via* making use of, benzoquinone, citric acid, and tert-butanol, respectively, to determine the principal oxidative species in the photocatalytic procedure. Therefore, we prepared 300 ml of MB with 20 ppm and add 3 mmol from one of the scavengers into the solution. Subsequently, we dispersed 0.03 g of photocatalyst and added it to the abovementioned solution. Afterward, we subjected our system to irradiation of UV, pipetted 4 ml of solution each 10 min, and separate catalyst from contaminant *via* centrifuging. We utilized a UV-spectrophotometer to monitor making process of each reaction.

To find out the effectiveness of synthesized materials to photocatalytically decolorize bacteria, Gram-positive *Staphylococcus aureus* (ATCC 6538), and Gram-negative *Escherichiacoli* (ATCC 25922) were selected to carry out pure culture investigation. First of all, we inoculated sterile 5 ml aliquots of Mueller Hinton broth (Merck) with *E. coli* and *S. aureus* and incubated overnight at 37°C. Next, we centrifuged them, washed with phosphate buffered saline (PBS) and adjusted appropriately their concentration. In order to evaluate the impact of Fe₃O₄/SiO₂/TiO₂ (N₁) and Fe₃O₄/SiO₂/TiO₂/CeVO₄ (N₅) on the chosen bacteria, 2% (w/w) suspensions of nanocomposites in Mueller Hinton (M-H) broth was prepared. The effect of Fe₃O₄/SiO₂/TiO₂ (N₁) and Fe₃O₄/SiO₂/TiO₂/CeVO₄ (N₅) nanocomposites on the behavior of *E. coli* and *S. aureus* was obtained by evaluating the growth of the cultures with photocatalysts compared to the growth of the culture in the medium. Mueller Hinton broth inoculated with bacteria only functioned as a positive control. For the test, sterile microtubes were filled with 0.5 ml of previously prepared solutions 1 mg. ml⁻¹ final concentration. Next, bacterial suspensions were added to each microtube (approximately 10⁵ colony-forming units/ml). The prepared systems were divided into three sets: we exposed the first set to the source of UV light (50W) for a period of 16 min and samples were taken at 0, 2, 4, 8, and 16 min. The second set was subjected to the source of visible light (Xe lamp) and we left the final set with no access to light for a

total period of 160 min. For evaluation, samples from the second and third groups were taken at 0, 20, 40, 80, and 160 min. The serial dilutions in PBS were prepared with achieved bacterial culture aliquots and the number of viable cells (CFU/ml) was assessed using the pour plate technique. All experiments were tested in triplicate.

Cell Culture

We prepared Panc1 cell lines from the National Cell Bank of Iran (NCBI, Tehran) and grew it in the RPMI 1640 medium (Gibco) added to 10% (v/v) Fetal Bovine Serum (FBS), penicillin/streptomycin (100 IU/ml, 100 µg/ml respectively) (Sigma, Germany). We incubated and kept cells in an atmosphere which has been humidified at 37°C and 5% CO₂. As soon as we reached 85% confluence, we rinsed cells with pure RPMI and gathered them *via* 0.25% Trypsin/EDTA solution (Sigma, Germany). All experiments were conducted three times. All experimental protocols were approved by the Baqiyatallah University of Medical Sciences Ethical Committee by letter IR.BMSU.REC.1397.409.

MTT Assay

The cytotoxicity effects of Fe₃O₄/SiO₂/TiO₂/CeVO₄ nanocomposite on Panc1 cells was evaluated using the MTT assay. This procedure is based on the potential of feasible cells to generate blue formazan crystals from yellow tetrazolium salt MTT *via* mitochondrial dehydrogenase. We positioned gathered cells in a plate with 96 cells (Nunc, Denmark) and density of 10⁴ cells/well. Next, we selected cells with varied concentrations of nanocomposites (2, 1, 0.5, 0.25, 0.125, 0.063, 0.0315, 0.0157 mg/ml), and incubated the microplate at 37°C and 5% CO₂ for one and two days. Afterward, we added 10 µl of MTT reagent to each well and incubated the plate for 4h. Next procedure was discarding of supernatants, adding 100 µl of the DMSO into each well, and incubating plates for 20 min, in sequence. Eventually, we managed to monitor cytotoxicity *via* evaluating the absorbance at an appropriate wavelength (λ = 570 nm) making use of ELISA plate reader (Lab System). The cell cytotoxicity and viability were computed, in terms of percentage, based on the following formula (Doosti et al., 2018):

$$\% \text{ Cytotoxicity} = 1 - \frac{\text{average absorbance of toxicant}}{\text{average absorbance of negative control}} \times 100 \quad (14)$$

RESULTS AND DISCUSSION

Characterization

The XRD plot of the Fe₃O₄ nanosized with pure phase cubic and space group of Fd-3m is revealed in **Figure 1A**. In this figure, there are a series of diffraction peaks at 35.60° ((311) line), and 63.10° ((220) line), which is in good agreement with Fe₃O₄ (JCPDS75-0449) and the calculated cell parameters of a = b = c = 8.3200 Å [5]. The XRD plot of the Fe₃O₄/SiO₂ nanostructure has appeared in **Figure 1B**. The Fe₃O₄/SiO₂ nanostructures are composed of two pure phases including Fe₃O₄ (JCPDS75-0449 and space group Fd-3m) as well as SiO₂ (JCPDS 75-1555 and space group P6222) that

show a series of diffraction peaks at the position of 26.13° with lines (101) which is well-matched with pure phase hexagonal Fe₃O₄ nanostructure. Besides, the XRD plot for Fe₃O₄/SiO₂ nanostructure prepared in room temperature with low crystallinity has been displayed in **Figure 1B** and the XRD plot of the Fe₃O₄/SiO₂/TiO₂ nanostructure have been shown in **Figure 1C**. The Fe₃O₄/SiO₂/TiO₂ nanostructures contain three pure phases such as Fe₃O₄ (JCPDS75-0449 and space group Fd-3m), SiO₂ (JCPDS 75-1555 and space group P6222) and TiO₂ (JCPDS 04-0477 and space group I41/amd) which indicate a series of diffraction peaks at the position of 25.32°, 27.52°, and 48.00° with lines (101), (004), and (200) which is compatible with pure phase of tetragonal TiO₂ nanostructures.

The XRD graph of the Fe₃O₄/SiO₂/TiO₂/CeVO₄ nanostructure has been demonstrated in **Figure 1D**. The Fe₃O₄/SiO₂/TiO₂/CeVO₄ nanostructures involve four pure phases like Fe₃O₄ (JCPDS75-0449 and space group Fd-3m), SiO₂ (JCPDS 75-1555 and space group P6222), TiO₂ (JCPDS 04-0477 and space group I41/amd), as well as CeVO₄ (JCPDS 084-1457 and space group I41/amd) suggesting a series of diffraction peaks at 24.03° Line (200), 32.04° Line (112) and 47.86° Line (312). One can simply find the good consistency between pure phases of tetragonal CeVO₄ nanostructure. Also, adding the CeVO₄ layer can result in decrease of intensity of three previous parts and therefore, the crystal size of nanocomposites have been increased.

Figure 2 shows the SEM images of synthesized Fe₃O₄/SiO₂/TiO₂ (N1) and optimum sample of Fe₃O₄/SiO₂/TiO₂/CeVO₄ (N5) nanoparticles under low and high magnification. The Fe₃O₄/SiO₂/TiO₂ nanoparticles with diameters of 50–70 nm and Fe₃O₄/SiO₂/TiO₂/CeVO₄ (N5) nanoparticles with diameters of 80–100 nm were found to be well synthesized. Morphologically, both of them have the same shape and uniform distribution. As well, TEM image of N₅ sample (**Figure 2E**) was taken where the darker regions shown in the photograph are related to the magnetic component and the brighter regions are related to the rest of the phases forming this nanostructure.

Also, investigate the phase of the optimum synthesized nanocomposite (N5), we further characterized the elements of synthesized nanocomposite using energy-dispersive X-ray spectroscopy (EDS) analyses. The EDS analysis confirmed the presence of the desired elements in the nanocomposite, as shown in **Figure 3**. To investigate the uniformity of the nanoparticles distribution, an elemental mapping analysis was conducted with EDS, as shown in **Figure 4**. The magnetic properties of the magnetic nanocomposites were measured using a vibrating sample magnetometer (VSM). **Figure 5** shows the room temperature magnetization curves of simple Fe₃O₄ nanoparticles, Fe₃O₄/SiO₂/TiO₂ nanocomposite (N₁) and the Fe₃O₄/SiO₂/TiO₂/CeVO₄ (N₅) samples. As illustrated in this figure, the saturation magnetizations (Ms) of the samples are 55.7, 25.3, and 9.2emu⁻¹, respectively. Our outcomes for the VSM analysis prove that the synthesized photocatalysts show typical superparamagnetic behavior. The reduction in the measured saturation magnetization is owing to the added next nanoparticles layers on Fe₃O₄.

We calculated the band gap based on a Tauc plot, a technique which is extensively utilized to obtain band gaps which have been

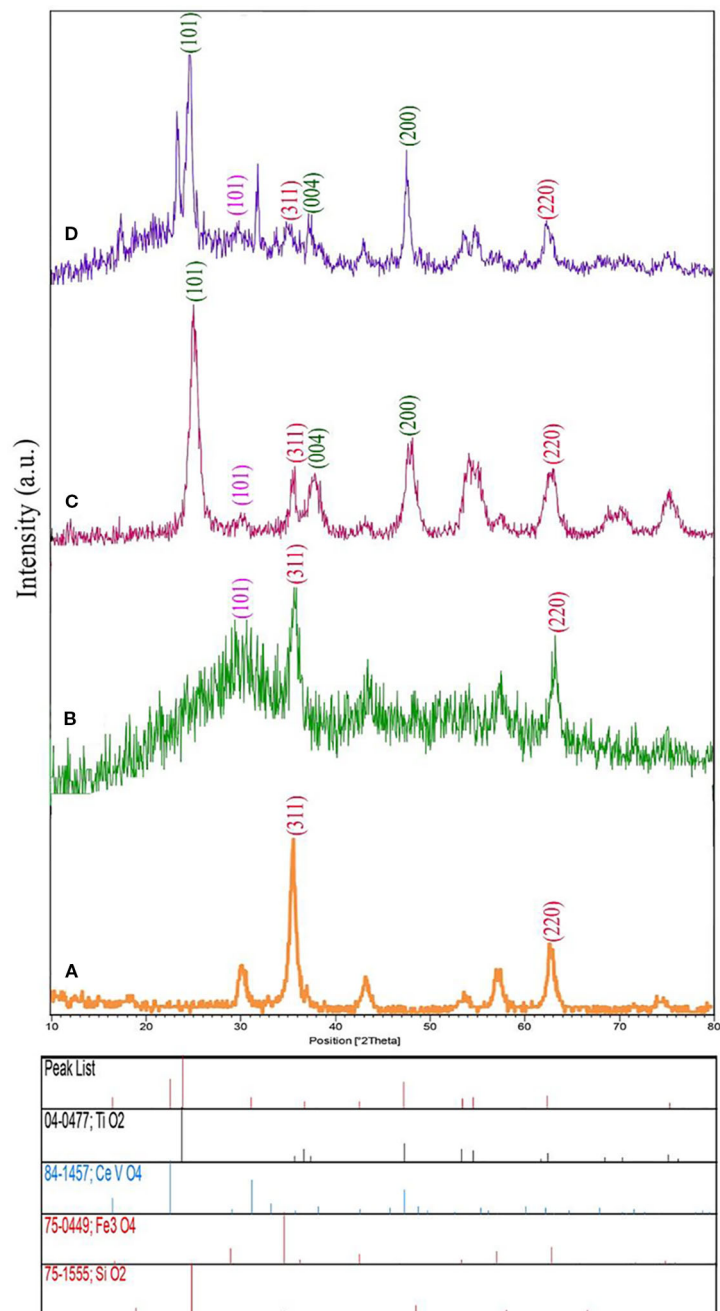


FIGURE 1 | X-ray diffraction (XRD) analysis of (A) Fe₃O₄ nanoparticles, (B) Fe₃O₄/SiO₂, and (C) Fe₃O₄/SiO₂/TiO₂ (N₁), and (D) Fe₃O₄/SiO₂/TiO₂/CeVO₄ (N₅) nanocomposites.

shown in **Figure 6**. The estimated band gap values (E_g) were 3.2, and 2.92 eV for the Fe₃O₄/SiO₂/TiO₂, and Fe₃O₄/SiO₂/TiO₂/CeVO₄ (N₅) samples, respectively.

Figure 7 shows the FTIR spectrum of Fe₃O₄ (a), Fe₃O₄/SiO₂ (b), Fe₃O₄/SiO₂/TiO₂ (N₁) (c), Fe₃O₄/SiO₂/TiO₂/CeVO₄ (N₅) (d), as well as N₅ sample after a complete photocatalytic reaction period with 20

ppm of MB dye. At all spectrums, the presence of water is shown by the appearance of the bending mode at around $\sim 1,600$ cm⁻¹ and the stretching mode at around $\sim 3,300$ cm⁻¹ (Kunarti et al., 2016; Doosti et al., 2018). A strong peak at ~ 588 cm⁻¹ of Fe₃O₄ was obtained which was assigned to the Fe-O stretching vibration. There was a new strong band around 1,087 cm⁻¹ in **Figure 7B** that came from

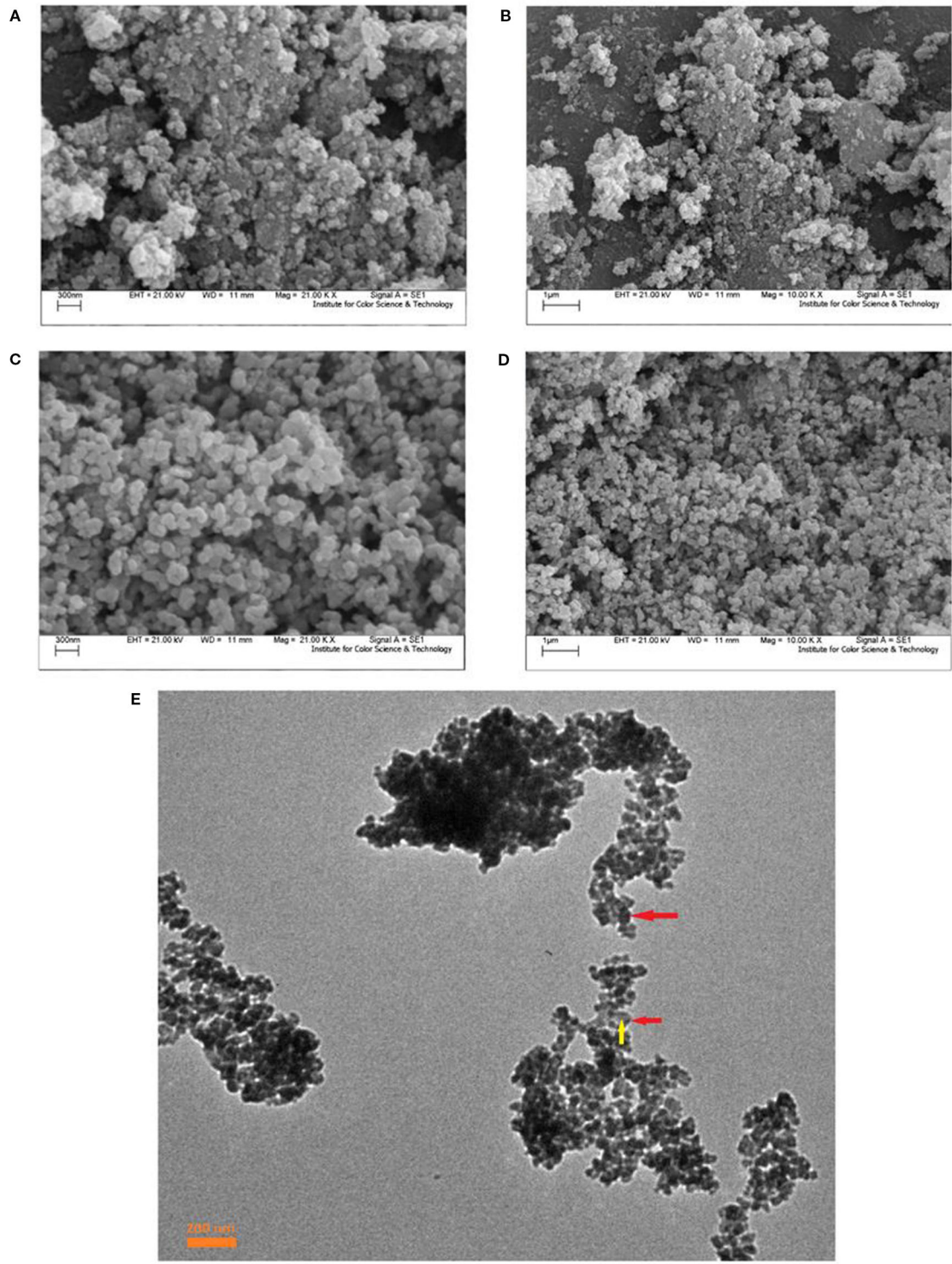


FIGURE 2 | Scanning electron microscopy (SEM) images of prepared nanocomposites; Fe₃O₄/SiO₂/TiO₂ (N₁) **(A, B)** Fe₃O₄/SiO₂/TiO₂/CeVO₄ (N₅); **(C, D)**, TEM image of N₅ sample **(E)**.

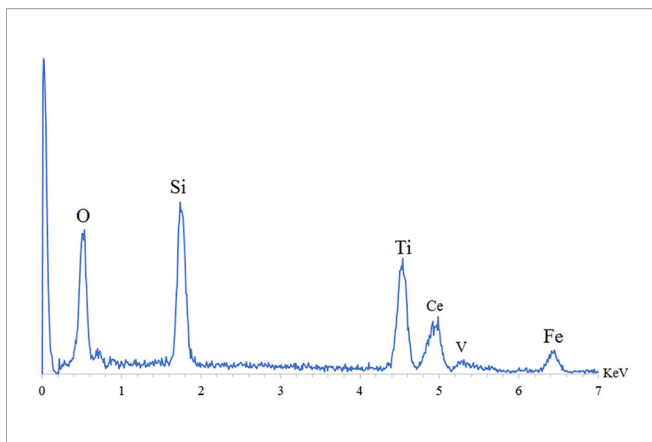


FIGURE 3 | Energy-dispersive X-ray spectroscopy (EDS) spectra of optimum sample Fe₃O₄/SiO₂/TiO₂/CeVO₄ (N₅).

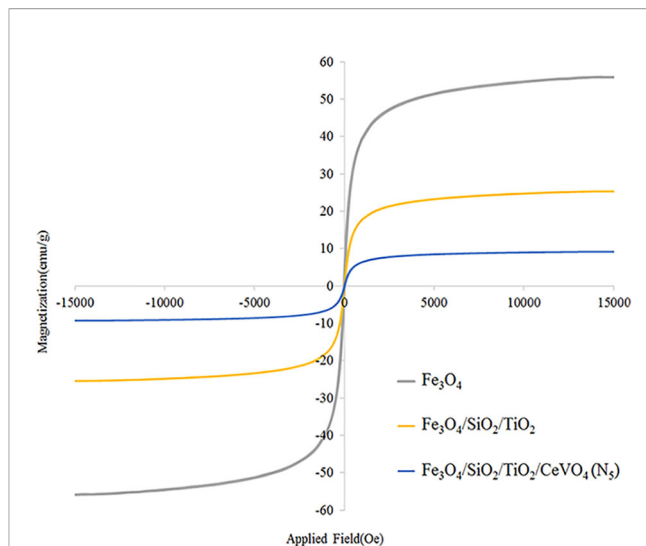


FIGURE 5 | Room temperature magnetization curve of Fe₃O₄ nanoparticles, Fe₃O₄/SiO₂/TiO₂ (N₅), and Fe₃O₄/SiO₂/TiO₂/CeVO₄ (N₅) nanocomposites.

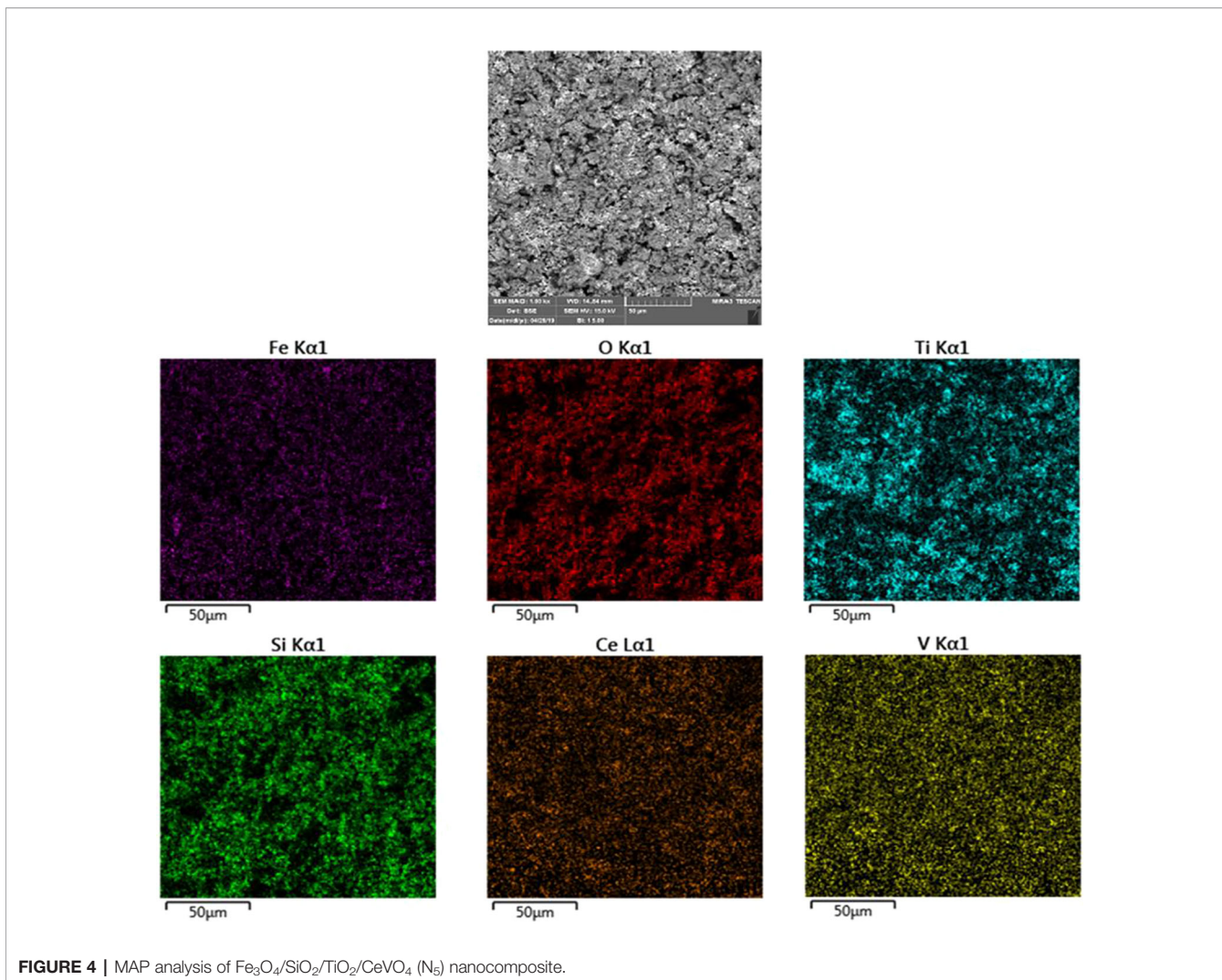


FIGURE 4 | MAP analysis of Fe₃O₄/SiO₂/TiO₂/CeVO₄ (N₅) nanocomposite.

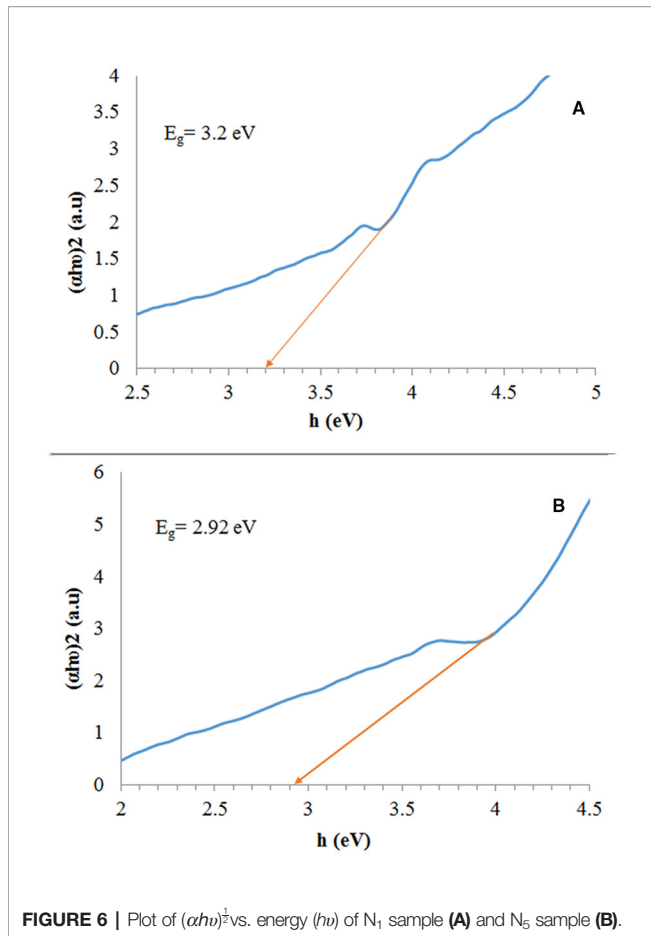


FIGURE 6 | Plot of $(\alpha h\nu)^2$ vs. energy ($h\nu$) of N₁ sample (A) and N₅ sample (B).

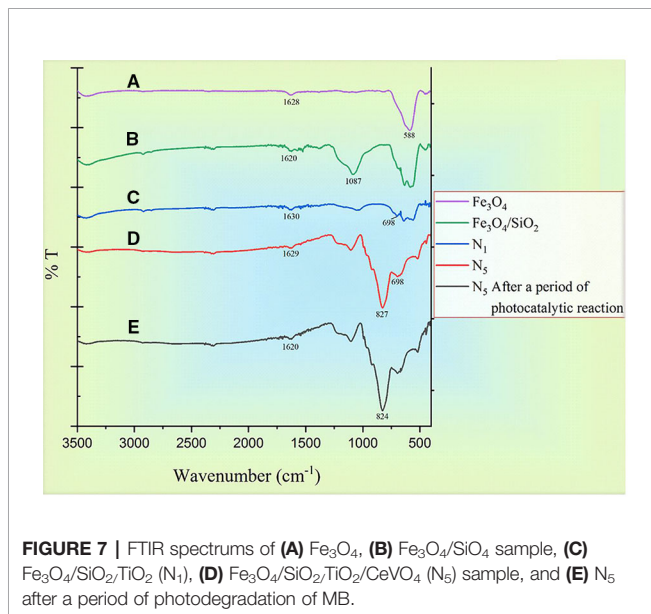


FIGURE 7 | FTIR spectrums of (A) Fe₃O₄, (B) Fe₃O₄/SiO₄ sample, (C) Fe₃O₄/SiO₂/TiO₂ (N₁), (D) Fe₃O₄/SiO₂/TiO₂/CeVO₄ (N₅) sample, and (E) N₅ after a period of photodegradation of MB.

the Si-O bond in SiO₂ (Kunarti et al., 2016) and the vibration band for the fingerprint of Ti-O-Ti bond in Figure 6C, which is located around 700 cm⁻¹ (Kunarti et al., 2016; Doosti et al., 2018). The presence of a strong peak at 827 cm⁻¹ is due to the V-O stretching vibration of VO₄ which has been displayed in Figure 7D (Marsooli et al., 2019). Figure 7E is related to the N₅ sample after a photocatalytic reaction period, which is in contrast to Figure 7D. Clearly, it has not changed to much extent and is slightly noisy, suggesting the synthesized nanocomposites did not absorb colored materials and have not been destroyed.

Photocatalytic Evaluation

The result of a photocatalytic test under the visible spectrum is shown in Figure 8. We conducted this test for all synthesized samples (N₁-N₅) by 20 ppm of MB (assisted by 1 ml/100 ml H₂O₂). Among all the tests performed within 100 min, it was found that the photocatalytic influence of N₅ sample (1:1.5 molar ratio) was higher than the rest of the specimens (Figure 8A). Figure 8B shows the Kinetic fit plot of -ln(C/C₀) vs. time for different synthesized photocatalysts to be pseudo-first order. The slope of the linear regression was utilized as the first order reaction rate constant.

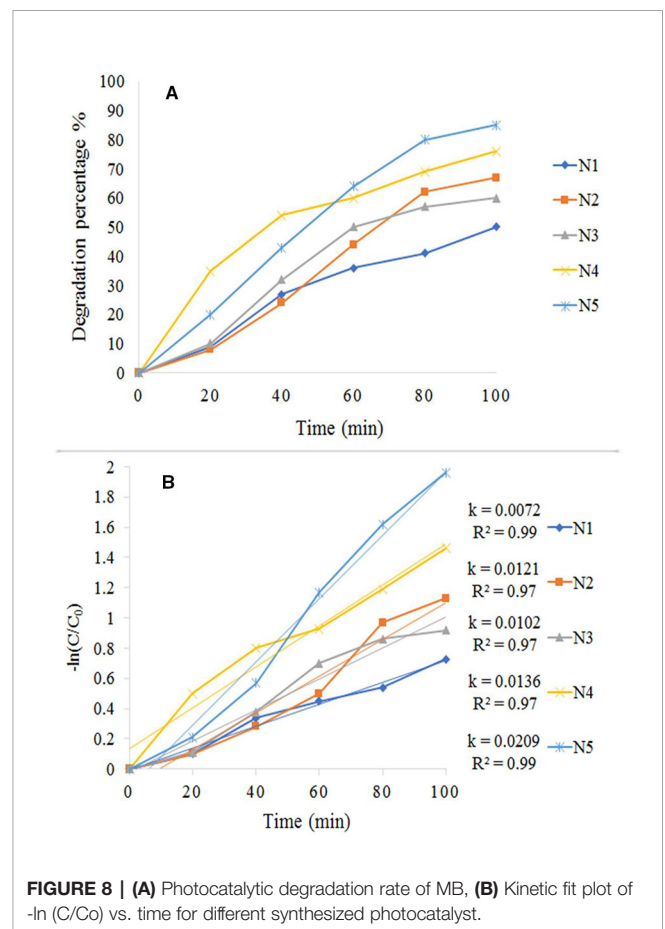


FIGURE 8 | (A) Photocatalytic degradation rate of MB, (B) Kinetic fit plot of -ln(C/C₀) vs. time for different synthesized photocatalyst.

TABLE 1 | Characterization comparison of Fe₃O₄/SiO₂/TiO₂/CeVO₄ (N₅) nanocomposite with other similar works.

Photocatalyst	Pollutant	Source of light	Radiation time (min)	Maximum destruction (%)	Reference
Polyaniline-modified Fe ₃ O ₄ /SiO ₂ /TiO ₂	MB	Visible	325	35	(Huang et al., 2011)
Fe ₃ O ₄ @SiO ₂ @TiO ₂ @Ho	MO	UV	150	80	(Mortazavi-Derazkola et al., 2017)
Fe ₃ O ₄ @SiO ₂ @TiO ₂ -Co/rGO	MB	Visible	160	100	(Fu et al., 2019)
Fe ₂ O ₃ -Fe ₃ O ₄ @SiO ₂ @TiO ₂ -TNS-GR	RhB	Visible	120	93	(Yang and Liu, 2019)
Fe ₃ O ₄ /SiO ₂ /TiO ₂ /CeVO ₄	MB	Visible	100	87	This work

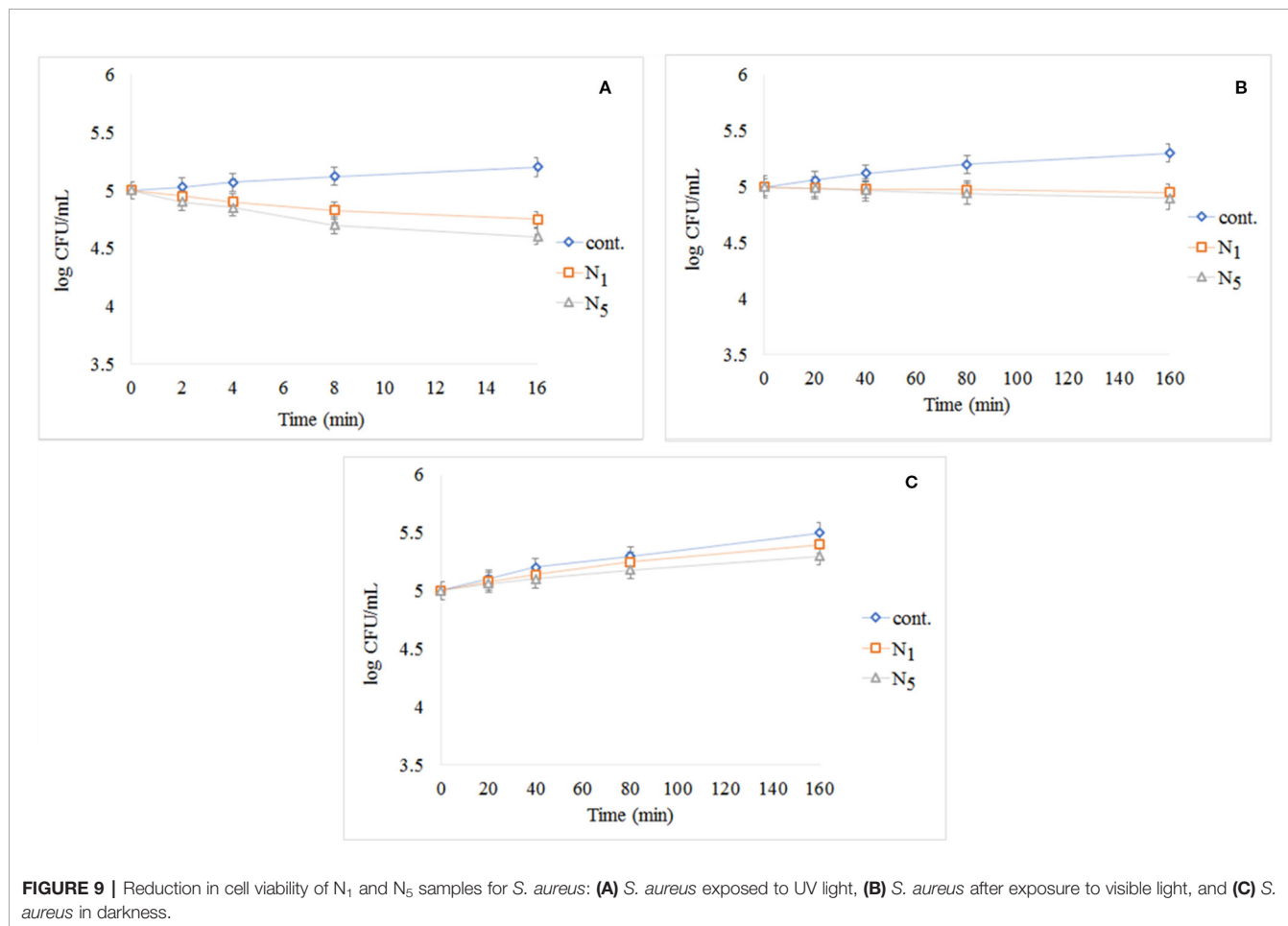
Eventually, N₅ sample showed the best performance and as a result, could be considered as a good candidate for the destruction of pollutants from the water. We have shown the efficiency of magnetic photocatalysts under visible and ultraviolet light in **Table 1**. According to the table, the degradation of organic dyes takes more time under visible light because the wavelengths of visible light have low energy. However, in this study, fabrication of Fe₃O₄/SiO₂/TiO₂/CeVO₄ nanocomposite for the first time, it was found that they have higher photocatalyst efficiency rather than other magnetic photocatalysts under visible light.

Photo Antibacterial Properties

Figure 9A shows the results of the test performed using *S. aureus* exposed to UV light. The cont. group had a small growth in comparison with N₁ and N₅ samples, and N₅ sample had better

performance. The results of the test performed using *S. aureus* exposed to visible light and dark condition respectively as illustrated in **Figures 9B, C**. As shown in **Figure 9B**, the control group has significantly increased by passing the time, but N₁ and N₅ samples have prevented the growth of bacteria. Also, seeing the growth for all samples in dark conditions demonstrates that the synthesized samples are light-dependent to take advantage of antibacterial properties.

The results of photo-antibacterial examination using *E. coli* has been shown in **Figure 10** by exposing to UV light (a), visible light (b), and dark condition (c). As can be seen in **Figure 10A**, the most decreased in the colony count is related to N₅ sample nanocomposite and there is no significant change in the control group observed during the test. The decrease of the bacteria was significant in comparison to cont. group. In **Figure 10B**, it was



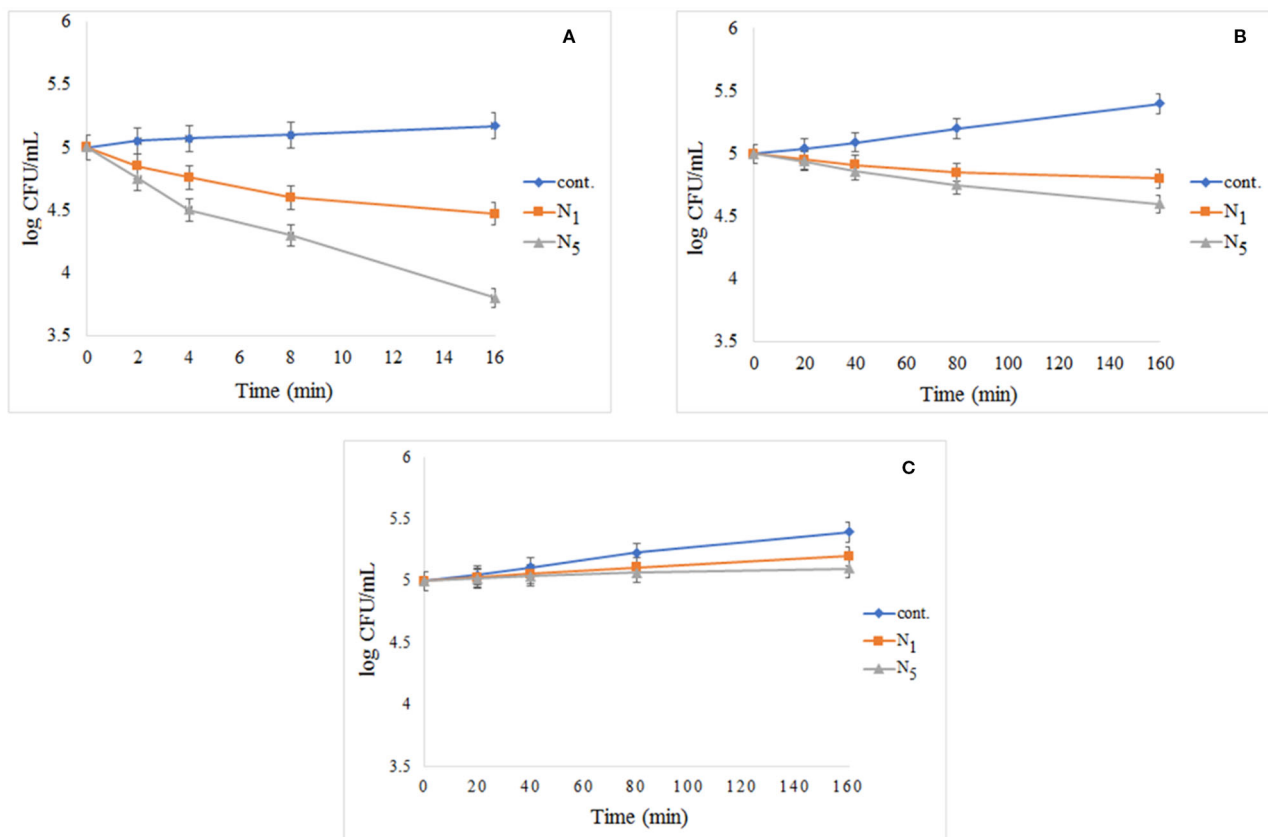


FIGURE 10 | Reduction in cell viability of N₁ and N₅ samples for *E. coli*: **(A)** *E. coli* exposed to UV light, **(B)** *E. coli* after exposure to visible light, and **(C)** *E. coli* without light access.

found that the cont. the group experienced significant growth under visible light by during the test, while the N₁ and N₅ nanocomposite decreased in compared to the cont. group and the N₅ sample showed the highest decrease. In **Figure 10C**, we found that all of the samples had experienced growth in darkness as time passes. This issue highlights the importance of light in the reaction system. As presented in the **Figure 10A**, the addition of a third phase (CeVO₄) to the nanocomposite has led to the elimination of more microorganisms.

Photodegradation Mechanism

To prove the presence of [•]OH in the Fe₃O₄/SiO₂/TiO₂/CeVO₄ (N₅) system during UV irradiation, [•]OH trapping PL experiments using terephthalic acid (TA) as a probe molecule were also carried out (**Figure 11**). As shown in **Figure 10B**, after irradiation for 150 s, the strong PL signal is seen at 425 nm, and the intensity significantly increased with the irradiation time as a comparison with dark treatment, which shows [•]OH radicals have been generated.

To study the photocatalytic degradation mechanism of Fe₃O₄/SiO₂/TiO₂/CeVO₄ nanocomposite, several agents were utilized to

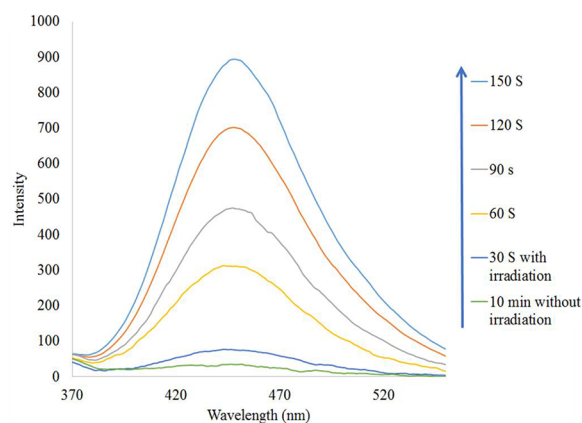
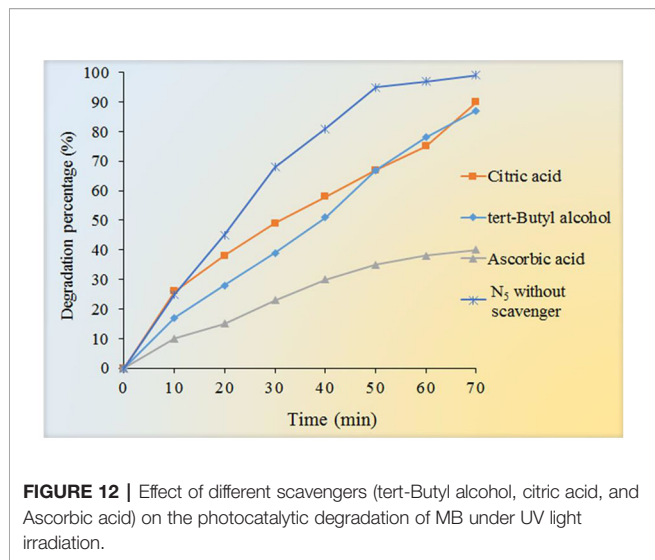


FIGURE 11 | [•]OH trapping PL spectra of Fe₃O₄/SiO₂/TiO₂/CeVO₄ (N₅) nanocomposite with TA solution under UV irradiation.

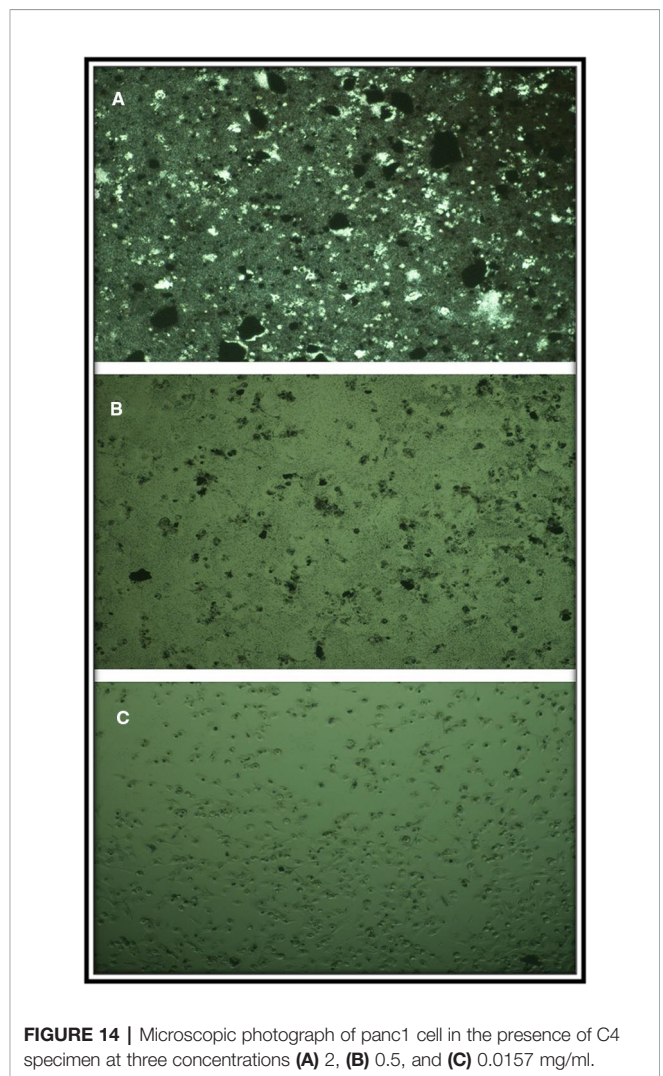
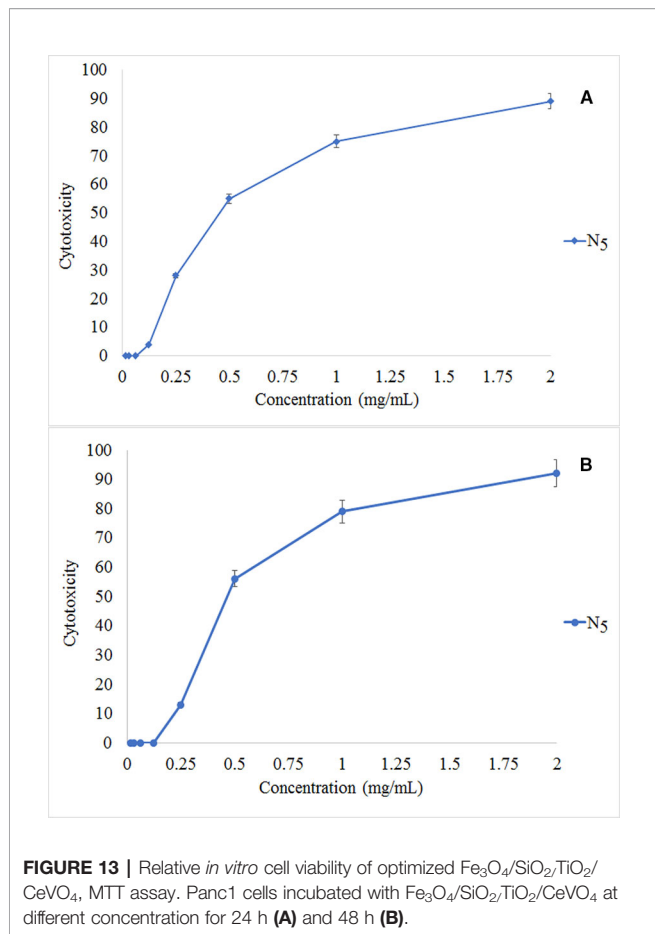


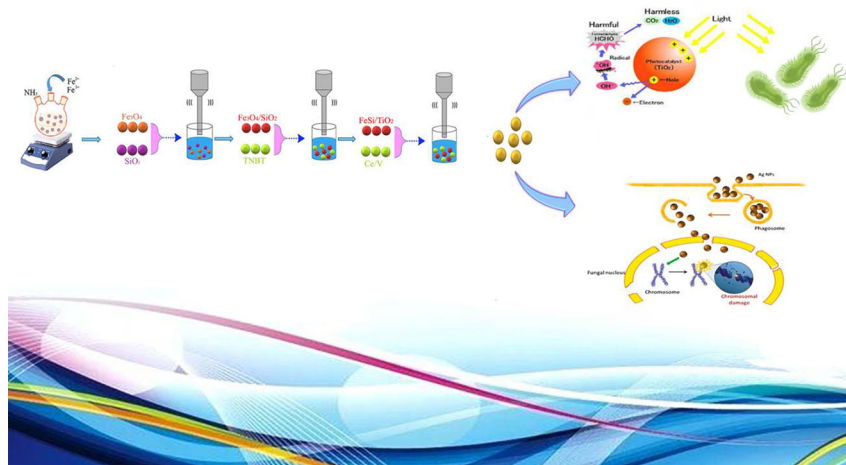
quench the relevant active species within the photocatalytic process, and the results are shown in **Figure 12**. In this study, t-butyl alcohol, Citric acid, and ascorbic acid were adopted to be the scavengers of hydroxyl radicals ([•]OH), holes (h⁺) and superoxide radical ([•]O₂⁻), respectively. As shown in **Figure 12**, when t-butyl alcohol and citric

acid were added to the reaction system, the photocatalytic efficiency was not noticeably changed but with the use of ascorbic acid, the reaction speed dropped sharply. However, when ascorbic acid was added to the reaction system, the photocatalytic efficiency was reduced from 99.9% to 38% for MB. Based on the results, we can conclude that [•]O₂⁻ is the major reactive species in the photodegradation of MB in the reaction system.

Cytotoxicity Effect

The MTT assay shows that C₄ nanocomposite had a toxic effect on a panc1 Cell line in a dose-dependent manner and its IC₅₀ is about 500 mg/L (**Figure 13**). The concentrations of N₅ sample used for photocatalytic properties are much lower than that of having toxic effects on mammalian cells. On the other hand, the time taken for the photocatalytic process was at most 160 min, while the effects of cytotoxicity have been investigated after 24 and 48 h. Also, **Figure 14** exhibits the microscopic photos of panc1 cells with optimized nanocomposite (N₅) at three different concentrations which confirm that once concentrations decrease, the toxicity of the N₅ sample is reduced as well.





SCHEME 1 | Schematic mechanism for the synthesis of Fe₃O₄/SiO₂/TiO₂/CeVO₄ and its different application.

CONCLUSIONS

Fe₃O₄/SiO₂/TiO₂ and Fe₃O₄/SiO₂/TiO₂/CeVO₄ nanocomposites were successfully synthesized in different molar ratios by Co-precipitation approach (assisted by ultrasonic method). Also, Schematic mechanism for the synthesis of Fe₃O₄/SiO₂/TiO₂/CeVO₄ and its different application is shown in **Scheme 1**. XRD, EDS, SEM, and FTIR methods confirmed the quality and presence of these nanocomposites. DRS data showed a significant decrease in the band gap by adding CeVO₄ to previous phases. From the photocatalytic test, it was found that the Fe₃O₄/SiO₂/TiO₂/CeVO₄ 1:1:1:2 is the optimized sample by photodegradation of methylene blue (~90% under visible light in 100 min). The photoantibacterial studies on *E. coli* and *S. aureus* by Fe₃O₄/SiO₂/TiO₂ and Fe₃O₄/SiO₂/TiO₂/CeVO₄ under dark conditions, UV, and visible light irradiation showed that the optimized nanocomposite had better efficiency than Fe₃O₄/SiO₂/TiO₂ and the cytotoxicity properties of the optimized sample were measured as well. In addition, it was found that the toxic effect on panc1 Cell line is in a dose-dependent manner and its IC₅₀ is approximately 500 mg/L.

REFERENCES

- Abbas, M., Rao, B. P., Islam, M. N., Naga, S., Takahashi, M., and Kim, C. (2014). Highly stable-silica encapsulating magnetite nanoparticles (Fe₃O₄/SiO₂) synthesized using single surfactantless-polyol process. *Ceram. Int.* 40 (1), 1379–1385. doi: 10.1016/j.ceramint.2013.07.019
- Absalan, F., and Nikazar, M. (2016). Application of response surface methodology for optimization of water treatment by Fe₃O₄/SiO₂/TiO₂ core-shell nanophotocatalyst. *Chem. Eng. Commun.* 203 (11), 1523–1531. doi: 10.1080/00986445.2016.1218335
- Barbusiński, K. (2005). The modified Fenton process for decolorization of dye wastewater. *Polish J. Environ. Stud.* 14 (3), 281–285.
- Basith, N. M., Vijaya, J. J., Kennedy, L. J., Bououdina, M., Jenefar, S., and Kaviyaran, V. (2014). Co-doped ZnO nanoparticles: structural, morphological, optical, magnetic and antibacterial studies. *J. Mater. Sci. Technol.* 30 (11), 1108–1117. doi: 10.1016/j.jmst.2014.07.013

DATA AVAILABILITY STATEMENT

The raw data supporting the conclusions of this article will be made available by the authors, without undue reservation, to any qualified researcher.

AUTHOR CONTRIBUTIONS

MM and AS contributed in conception, design, statistical analysis and drafting of the manuscript. MR-M, MF-R, KA, ME-A, FA, ES, SM, MG, HE, and YJ contributed in data collection and manuscript drafting. All authors approved the final version for submission.

ACKNOWLEDGMENTS

Authors are grateful to the council of *Kashan University of Medical Sciences* for providing financial support to undertake this work. This work was supported by the Council of *Kashan University of Medical Sciences* by Grant Conception No. 97022960.

- Carp, O., Huisman, C. L., and Reller, A. (2004). Photoinduced reactivity of titanium dioxide. *Prog. In Solid state Chem.* 32 (1-2), 33–177. doi: 10.1016/j.progsolidstchem.2004.08.001
- Dogan, D., and Turkdemir, H. (2012). Electrochemical treatment of actual textile indigo dye effluent. *Polish J. Environ. Stud.* 21 (5).
- Doosti, M.-H., Ahmadi, K., and Fasihi-Ramandi, M. (2018). The effect of ethanolic extract of *Thymus kotschyanus* on cancer cell growth *in vitro* and depression-like behavior in the mouse. *J. Tradit. Complementary Med.* 8 (1), 89–94. doi: 10.1016/j.jtcm.2017.03.003
- Eghbali-Arani, M., Sobhani-Nasab, A., Rahimi-Nasrabadi, M., and Pourmasoud, S. (2018). Green synthesis and characterization of SmVO₄ nanoparticles in the presence of carbohydrates as capping agents with investigation of visible-light photocatalytic properties. *J. Electro. Mater.* 47 (7), 3757–3769. doi: 10.1007/s11664-018-6236-3
- Ezhilarasi, A. A., Vijaya, J. J., Kaviyaran, K., Maaza, M., Ayeshamariam, A., and Kennedy, L. J. (2016). Green synthesis of NiO nanoparticles using Moringa

- oleifera extract and their biomedical applications: cytotoxicity effect of nanoparticles against HT-29 cancer cells. *J. Photochem. Photobiol. B: Biol.* 164, 352–360. doi: 10.1016/j.jphotobiol.2016.10.003
- Ezhilarasi, A. A., Vijaya, J. J., Kaviyarasu, K., Kennedy, L. J., Ramalingam, R. J., and Al-Lohedan, H. A. (2018). Green synthesis of NiO nanoparticles using Aegle marmelos leaf extract for the evaluation of in-vitro cytotoxicity, antibacterial and photocatalytic properties. *J. Photochem. Photobiol. B: Biol.* 180, 39–50. doi: 10.1016/j.jphotobiol.2018.01.023
- Farré, M. J., Franch, M. I., Malato, S., Ayllón, J. A., Peral, J., and Doménech, X. (2005). Degradation of some biorecalcitrant pesticides by homogeneous and heterogeneous photocatalytic ozonation. *Chemosphere* 58 (8), 1127–1133. doi: 10.1016/j.chemosphere.2004.09.064
- Foster, H. A., Ditta, I. B., Varghese, S., and Steele, A. (2011). Photocatalytic disinfection using titanium dioxide: spectrum and mechanism of antimicrobial activity. *Appl. Microbiol. Biotechnol.* 90 (6), 1847–1868. doi: 10.1007/s00253-011-3213-7
- Fu, C., Liu, X., Wang, Y., Li, L., and Zhang, Z. (2019). Preparation and characterization of Fe₃O₄@SiO₂@TiO₂-Co/rGO magnetic visible light photocatalyst for water treatment. *RSC Adv.* 9 (35), 20256–20265. doi: 10.1039/C9RA04002A
- Hassan, N., Jalil, A., Khusnun, N., Ali, M., and Haron, S. (2019). Role of reduced graphene oxide in improving interfacial charge transfer of hybridized rGO/silica/zirconia for enhanced Bisphenol A photodegradation. *J. Alloys Compd.* 789, 221–230. doi: 10.1016/j.jallcom.2019.03.105
- Hosseinpour-Mashkani, S. S., and Sobhani-Nasab, A. (2017). Investigation the effect of temperature and polymeric capping agents on the size and photocatalytic properties of NdVO₄ nanoparticles. *J. Mater. Sci.: Mater. Electron.* 28 (21), 16459–16466.
- Huang, X., Wang, G., Yang, M., Guo, W., and Gao, H. (2011). Synthesis of polyaniline-modified Fe₃O₄/SiO₂/TiO₂ composite microspheres and their photocatalytic application. *Mater. Lett.* 65 (19–20), 2887–2890. doi: 10.1016/j.matlet.2011.06.005
- Ide, Y., Liu, F., Zhang, J., Kawamoto, N., Komaguchi, K., Bando, Y., et al. (2014). Hybridization of Au nanoparticle-loaded TiO₂ with BN nanosheets for efficient solar-driven photocatalysis. *J. Mater. Chem. A* 2 (12), 4150–4156. doi: 10.1039/c3ta13769d
- Ioannou, L., Michael, C., Vakondios, N., Drosou, K., Xekoukoulotakis, N. P., Diamadopoulos, E., et al. (2013). Winery wastewater purification by reverse osmosis and oxidation of the concentrate by solar photo-Fenton. *Sep. Purif. Technol.* 118, 659–669. doi: 10.1016/j.seppur.2013.07.049
- Jayaprakash, N., Vijaya, J. J., Kennedy, L. J., Priadharsini, K., and Palani, P. (2015). Antibacterial activity of silver nanoparticles synthesized from serine. *Mater. Sci. Eng.: C* 49, 316–322. doi: 10.1016/j.msec.2015.01.012
- Jayaprakash, N., Vijaya, J. J., Kaviyarasu, K., Kombaiyah, K., Kennedy, L. J., Ramalingam, R. J., et al. (2017). Green synthesis of Ag nanoparticles using Tamarind fruit extract for the antibacterial studies. *J. Photochem. Photobiol. B: Biol.* 169, 178–185. doi: 10.1016/j.jphotobiol.2017.03.013
- Jesudoss, S., Vijaya, J. J., Kennedy, L. J., Rajan, P. I., Al-Lohedan, H. A., Ramalingam, R. J., et al. (2016). Studies on the efficient dual performance of Mn_{1-x}Ni_xFe₂O₄ spinel nanoparticles in photodegradation and antibacterial activity. *J. Photochem. Photobiol. B: Biol.* 165, 121–132. doi: 10.1016/j.jphotobiol.2016.10.004
- Jesudoss, S., Vijaya, J. J., Rajan, P. I., Kaviyarasu, K., Sivachidambaram, M., Kennedy, L. J., et al. (2017). High performance multifunctional green Co₃O₄ spinel nanoparticles: photodegradation of textile dye effluents, catalytic hydrogenation of nitro-aromatics and antibacterial potential. *Photochem. Photobiol. Sci.* 16 (5), 766–778. doi: 10.1039/C7PP00006E
- Kim, S., and Choi, W. (2002). Kinetics and mechanisms of photocatalytic degradation of (CH₃)_nNH₄ⁿ⁺ (0 ≤ n ≤ 4) in TiO₂ suspension: the role of OH radicals. *Environ. Sci. Technol.* 36 (9), 2019–2025. doi: 10.1021/es015560s
- Kooshki, H., Sobhani-Nasab, A., Eghbali-Arani, M., Ahmadi, F., Ameri, V., and Rahimi-Nasrabadi, M. (2019). Eco-friendly synthesis of PbTiO₃ nanoparticles and PbTiO₃/carbon quantum dots binary nano-hybrids for enhanced photocatalytic performance under visible light. *Sep. Purif. Technol.* 211, 873–881. doi: 10.1016/j.seppur.2018.10.057
- Kowalski, Z., Kaczmarek, S., Drozdowski, W., Witkowski, M., Makowski, M., Brylew, K., et al. (2018). Radioluminescence, low temperature thermoluminescence and scintillation properties of Ca and Eu doped ZnWO₄ single crystals. *Radiat. Meas.* 118, 1–7. doi: 10.1016/j.radmeas.2018.08.002
- Kubacka, A., Diez, M. S., Rojo, D., Bargiela, R., Ciordia, S., Zapico, I., et al. (2014). Understanding the antimicrobial mechanism of TiO₂-based nanocomposite films in a pathogenic bacterium. *Sci. Rep.* 4, 4134. doi: 10.1038/srep04134
- Kunarti, E., Syoufan, A., Budi, I., and Pradipta, A. (2016). Preparation and properties of Fe₃O₄/SiO₂/TiO₂ core-shell nanocomposite as recoverable photocatalyst. *Asian J. Chem.* 28 (6), 1343–1346. doi: 10.14233/ajchem.2016.19697
- Lin, Y., Geng, Z., Cai, H., Ma, L., Chen, J., Zeng, J., et al. (2012). Ternary graphene-TiO₂-Fe₃O₄ nanocomposite as a collectable photocatalyst with enhanced durability. *Eur. J. Inorg. Chem.* 2012 (28), 4439–4444.
- Liu, H., Li, G., Qu, J., and Liu, H. (2007). Degradation of azo dye acid orange 7 in water by Fe₀/granular activated carbon system in the presence of ultrasound. *J. Hazard. Mater.* 144 (1–2), 180–186. doi: 10.1016/j.jhazmat.2006.10.009
- Liu, S., Yang, M.-Q., Tang, Z.-R., and Xu, Y.-J. (2014). A nanotree-like CdS/ZnO nanocomposite with spatially branched hierarchical structure for photocatalytic fine-chemical synthesis. *Nanoscale* 6 (13), 7193–7198. doi: 10.1039/c4nr01227e
- Maleki, A., and Kamalzare, M. (2014). An efficient synthesis of benzodiazepine derivatives via a one-pot, three-component reaction accelerated by a chitosan-supported superparamagnetic iron oxide nanocomposite. *Tetrahedron Lett.* 55 (50), 6931–6934. doi: 10.1016/j.tetlet.2014.10.120
- Maleki, A., Rabbani, M., and Shahrokh, S. (2015). Preparation and characterization of a silica-based magnetic nanocomposite and its application as a recoverable catalyst for the one-pot multicomponent synthesis of quinazolinone derivatives. *Appl. Organomet. Chem.* 29 (12), 809–814. doi: 10.1002/aoc.3373
- Maleki, A., Aghaei, M., and Ghamari, N. (2016a). Facile synthesis of tetrahydrobenzoxanthenones via a one-pot three-component reaction using an eco-friendly and magnetized biopolymer chitosan-based heterogeneous nanocatalyst. *Appl. Organomet. Chem.* 30 (11), 939–942. doi: 10.1002/aoc.3524
- Maleki, A., Rahimi, R., and Maleki, S. (2016b). Efficient oxidation and epoxidation using a chromium (VI)-based magnetic nanocomposite. *Environ. Chem. Lett.* 14 (2), 195–199. doi: 10.1007/s10311-016-0558-2
- Maleki, A., Aghaei, M., Hafizi-Atabak, H. R., and Ferdowsi, M. (2017). Ultrasonic treatment of CoFe₂O₄ B₂O₃-SiO₂ as a new hybrid magnetic composite nanostructure and catalytic application in the synthesis of dihydroquinazolinones. *Ultrason. Sonochem.* 37, 260–266. doi: 10.1016/j.ultrsonch.2017.01.022
- Maleki, A., Niksefat, M., Rahimi, J., and Azadegan, S. (2019b). Facile synthesis of tetrazolo [1, 5-a] pyrimidine with the aid of an effective gallic acid nanomagnetic catalyst. *Polyhedron* 167, 103–110. doi: 10.1016/j.poly.2019.04.015
- Maleki, A., Taheri-Ledari, R., Rahimi, J., Soroushnejad, M., and Hajizadeh, Z. (2019c). Facile peptide bond formation: effective interplay between isothiazolone rings and silanol groups at silver/iron oxide nanocomposite surfaces. *ACS Omega* 4 (6), 10629–10639. doi: 10.1021/acsomega.9b00986
- Maleki, A., Aghaei, M., and Kari, T. (2019a). Facile Synthesis of 7-Aryl-benzo [h] tetrazolo [5, 1-b] quinazolinone-5, 6-dione fused polycyclic compounds by using a novel magnetic polyurethane catalyst. *Polycyclic Aromat. Compd.* 39 (3), 266–278. doi: 10.1080/10406638.2017.1325746
- Maleki, A., Varzi, Z., and Hassanzadeh-Afruzi, F. (2019d). Preparation and characterization of an eco-friendly ZnFe₂O₄@alginate nanocomposite catalyst and its application in the synthesis of 2-amino-3-cyano-4H-pyran derivatives. *Polyhedron* 171, 193–202. doi: 10.1016/j.poly.2019.07.016
- Marsooli, M. A., Fasihi-Ramandi, M., Adib, K., Pourmasoud, S., Ahmadi, F., Ganjali, M. R., et al. (2019). Preparation and Characterization of Magnetic Fe₃O₄/CdWO₄ and Fe₃O₄/CdWO₄/PrVO₄ nanoparticles and investigation of their photocatalytic and anticancer properties on PANC1 cells. *Materials* 12 (19), 3274. doi: 10.3390/ma12193274
- Mortazavi-Derazkola, S., Salavati-Niasari, M., Amiri, O., and Abbasi, A. (2017). Fabrication and characterization of Fe₃O₄@SiO₂@TiO₂@Ho nanostructures as a novel and highly efficient photocatalyst for degradation of organic pollution. *J. Energy Chem.* 26 (1), 17–23. doi: 10.1016/j.jechem.2016.10.015
- Peymani-Motlagh, S. M., Moeinian, N., Rostami, M., Fasihi-Ramandi, M., Sobhani-Nasab, A., Rahimi-Nasrabadi, M., et al. (2019a). Effect of Gd³⁺, Pr³⁺-or Sm³⁺-substituted cobalt-zinc

- ferrite on photodegradation of methyl orange and cytotoxicity tests. *J. Rare Earths*. 37 (12), 1288–1295. doi: 10.1016/j.jre.2019.04.010
- Peymani-Motlagh, S. M., Sobhani-Nasab, A., Rostami, M., Sobati, H., Eghbali-Arani, M., Fasihi-Ramandi, M., et al. (2019b). Assessing the magnetic, cytotoxic and photocatalytic influence of incorporating Yb³⁺ or Pr³⁺ ions in cobalt–nickel ferrite. *J. Mater. Sci.: Mater. Electron.* 30 (7), 6902–6909. doi: 10.1007/s10854-019-01005-9
- Rahimi-Nasrabadi, M., Pourmortazavi, S. M., Ganjali, M. R., Norouzi, P., Faridbod, F., and Karimi, M. S. (2016a). Statistically optimized synthesis of dyspersium tungstate nanoparticles as photocatalyst. *J. Mater. Sci.: Mater. Electron.* 27 (12), 12860–12868. doi: 10.1007/s10854-016-5421-5
- Rahimi-Nasrabadi, M., Ahmadi, F., and Eghbali-Arani, M. (2016b). Simple morphology-controlled fabrication of CdTiO₃ nanoparticles with the aid of different capping agents. *J. Mater. Sci.: Mater. Electron.* 27 (12), 13294–13299. doi: 10.1007/s10854-016-5478-1
- Rahimi-Nasrabadi, M., Ghaderi, A., Banafshe, H. R., Eghbali-Arani, M., Akbari, M., Ahmadi, F., et al. (2019). Preparation of Co₂TiO₄/CoTiO₃/Polyaniline ternary nano-hybrids for enhanced destruction of agriculture poison and organic dyes under visible-light irradiation. *J. Mater. Sci.: Mater. Electron.* 30 (17), 15854–15868.
- Rajan, P. I., Vijaya, J. J., Jesudoss, S., Kaviyarasu, K., Kennedy, L. J., Jothiramalngam, R., et al. (2017). Green-fuel-mediated synthesis of self-assembled NiO nano-sticks for dual applications—photocatalytic activity on Rose Bengal dye and antimicrobial action on bacterial strains. *Mater. Res. Express* 4 (8), 085030.
- Rashid, J., Barakat, M., Ruzmanova, Y., and Chianese, A. (2015). Fe₃O₄/SiO₂/TiO₂ nanoparticles for photocatalytic degradation of 2-chlorophenol in simulated wastewater. *Environ. Sci. Pollut. Res.* 22 (4), 3149–3157. doi: 10.1007/s11356-014-3598-9
- Sangsefidi, F. S., Nejati, M., Verdi, J., and Salavati-Niasari, M. (2017). Green synthesis and characterization of cerium oxide nanostructures in the presence carbohydrate sugars as a capping agent and investigation of their cytotoxicity on the mesenchymal stem cell. *J. Cleaner Prod.* 156, 741–749. doi: 10.1016/j.jclepro.2017.04.114
- Sedighi, F., Esmaili-Zare, M., Sobhani-Nasab, A., and Behpour, M. (2018). Synthesis and characterization of CuWO₄ nanoparticle and CuWO₄/NiO nanocomposite using co-precipitation method; application in photodegradation of organic dye in water. *J. Mater. Sci.: Mater. In Electron.* 29 (16), 13737–13745.
- Shi, W., Guo, F., and Yuan, S. (2017). In situ synthesis of Z-scheme Ag₃PO₄/CuBi₂O₄ photocatalysts and enhanced photocatalytic performance for the degradation of tetracycline under visible light irradiation. *Appl. Catal. B.: Environ.* 209, 720–728. doi: 10.1016/j.apcatb.2017.03.048
- Sobhani-Nasab, A., and Sadeghi, M. (2016). Preparation and characterization of calcium tungstate nanoparticles with the aid of amino acids and investigation its photocatalytic application. *J. Mater. Sci.: Mater. Electron.* 27 (8), 7933–7938. doi: 10.1007/s10854-016-4785-x
- Sobhani-Nasab, A., Behvandi, S., Karimi, M. A., Sohoul, E., Karimi, M. S., Gholipour, N., et al. (2019a). Synergetic effect of graphene oxide and C₃N₄ as co-catalyst for enhanced photocatalytic performance of dyes on Yb₂(MoO₄)₃/YbMoO₄ nanocomposite. *Ceram. Int.* 17847–17858. doi: 10.1016/j.ceramint.2019.05.356
- Sobhani-Nasab, A., Behpour, M., Rahimi-Nasrabadi, M., Ahmadi, F., Pourmasoud, S., and Sedighi, F. (2019b). Preparation, characterization and investigation of sonophotocatalytic activity of thulium titanate/polyaniline nanocomposites in degradation of dyes. *Ultrason. Sonochem.* 50, 46–58. doi: 10.1016/j.ultrsonch.2018.08.021
- Sobhani-Nasab, A., Behpour, M., Rahimi-Nasrabadi, M., Ahmadi, F., and Pourmasoud, S. (2019c). New method for synthesis of BaFe₁₂O₁₉/Sm₂Ti₂O₇ and BaFe₁₂O₁₉/Sm₂Ti₂O₇/Ag nano-hybrid and investigation of optical and photocatalytic properties. *J. Mater. Sci.: Mater. Electron.* 30 (6), 5854–5865. doi: 10.1007/s10854-019-00883-3
- Sobhani-Nasab, A., Pourmasoud, S., Ahmadi, F., Wysokowski, M., Jesionowski, T., Ehrlich, H., et al. (2019d). Synthesis and characterization of MnWO₄/TmVO₄ ternary nano-hybrids by an ultrasonic method for enhanced photocatalytic activity in the degradation of organic dyes. *Mater. Lett.* 238, 159–162. doi: 10.1016/j.matlet.2018.11.175
- Su, W., Zhang, T., Li, L., Xing, J., He, M., Zhong, Y., et al. (2014). Synthesis of small yolk–shell Fe₃O₄@TiO₂ nanoparticles with controllable thickness as recyclable photocatalysts. *RSC Adv.* 4 (17), 8901–8906. doi: 10.1039/c3ra47461e
- Subramanian, V., Wolf, E. E., and Kamat, P. V. (2004). Catalysis with TiO₂/gold nanocomposites. effect of metal particle size on the fermi level equilibration. *J. Am. Chem. Soc.* 126 (15), 4943–4950.
- Suresh, P., Vijaya, J. J., and Kennedy, L. J. (2014). Photocatalytic degradation of textile-dyeing wastewater by using a microwave combustion-synthesized zirconium oxide supported activated carbon. *Mater. Sci. Semicond. Process.* 27, 482–493. doi: 10.1016/j.mssp.2014.06.050
- Suresh, P., Vijaya, J. J., Balasubramaniam, T., and John Kennedy, L. (2016). Synergy effect in the photocatalytic degradation of textile dyeing waste water by using microwave combustion synthesized nickel oxide supported activated carbon. *Desalin. Water Treat* 57 (8), 3766–3781. doi: 10.1080/19443994.2014.989276
- Vijaya, J. J., Jayaprakash, N., Kombaiyah, K., Kaviyarasu, K., Kennedy, L. J., Ramalingam, R. J., et al. (2017). Bioreduction potentials of dried root of Zingiber officinale for a simple green synthesis of silver nanoparticles: antibacterial studies. *J. Photochem. Photobiol. B.: Biol.* 177, 62–68. doi: 10.1016/j.jphotobiol.2017.10.007
- Wei, Y., Han, B., Hu, X., Lin, Y., Wang, X., and Deng, X. (2012). Synthesis of Fe₃O₄ nanoparticles and their magnetic properties. *Proc. Eng.* 27, 632–637. doi: 10.1016/j.proeng.2011.12.498
- Xing, Z., Zhou, W., Du, F., Qu, Y., Tian, G., Pan, K., et al. (2014). A floating macro/mesoporous crystalline anatase TiO₂ ceramic with enhanced photocatalytic performance for recalcitrant wastewater degradation. *Dalton Trans.* 43 (2), 790–798. doi: 10.1039/C3DT52433G
- Yang, W., and Liu, X. (2019). A novel Fe₂O₃-Fe₃O₄@SiO₂/TiO₂-TNS-GR magnetic composite with an enhanced visible photocatalytic property. *Funct. Mater. Lett.* 12, 1–4. doi: 10.1142/S1793604719500061
- Yu, J., Dai, G., and Huang, B. (2009). Fabrication and characterization of visible-light-driven plasmonic photocatalyst Ag/AgCl/TiO₂ nanotube arrays. *J. Phys. Chem. C*. 113 (37), 16394–16401. doi: 10.1021/jp905247j
- Zhang, Q., Gao, L., and Guo, J. (2000). Effects of calcination on the photocatalytic properties of nanosized TiO₂ powders prepared by TiCl₄ hydrolysis. *Appl. Catal. B.: Environ.* 26 (3), 207–215. doi: 10.1016/S0926-3373(00)00122-3
- Zhang, L., Chen, J., Yu, W., Zhao, Q., and Liu, J. (2018). Antimicrobial nanocomposites prepared from montmorillonite/Ag. *J. Nanomater.* 2018.
- Zheng, W., Zou, Y., Li, X., and Machesky, M. L. (2013). Fate of estrogen conjugate 17 α -estradiol-3-sulfate in dairy wastewater: comparison of aerobic and anaerobic degradation and metabolite formation. *J. Hazard. Mater.* 258, 109–115. doi: 10.1016/j.jhazmat.2013.04.038

Conflict of Interest: The authors declare that the research was conducted in the absence of any commercial or financial relationships that could be construed as a potential conflict of interest.

Copyright © 2020 Marsooli, Rahimi-Nasrabadi, Fasihi-Ramandi, Adib, Eghbali-Arani, Ahmadi, Sohoul, Sobhani nasab, Mirhosseini, Gangali, Ehrlich and Joseph. This is an open-access article distributed under the terms of the Creative Commons Attribution License (CC BY). The use, distribution or reproduction in other forums is permitted, provided the original author(s) and the copyright owner(s) are credited and that the original publication in this journal is cited, in accordance with accepted academic practice. No use, distribution or reproduction is permitted which does not comply with these terms.